Theory of Fe, Co, Ni, Cu, and their complexes with hydrogen in ZnO

M. G. Wardle, J. P. Goss, and P. R. Briddon
School of Natural Sciences, University of Newcastle upon Tyne, Newcastle upon Tyne NE1 7RU, United Kingdom
(Received 22 June 2005; published 11 October 2005)

The properties of a range of 3*d* transition metals and their complexes with hydrogen are studied using local-density-functional methods. The location of the impurity-related 3*d* bands strongly affects the electronic and magnetic properties of both substitutional and interstitial impurities, with high spins being preferred in line with Hund's rule. The relative formation energies of the defects are considered and the favorable defect for various growth conditions under equilibrium discerned, indicating strongly bound impurity pairs and impurity-hydrogen complexes. H-related local vibrational modes are compared with experimental observations, and in particular models proposed in the literature for Cu—H complexes have been examined.

DOI: 10.1103/PhysRevB.72.155108 PACS number(s): 71.55.Gs, 71.15.Nc, 61.72.Vv, 61.72.Bb

I. INTRODUCTION

ZnO has become a prominent material for wide-gap semiconductor, optoelectronic, and, via doping with transition metals (TM's), spintronics applications.[1–4]

TM's are common impurities in as-grown ZnO. Fe, Co, Ni, and Cu exist in the 2+ oxidation state with Co_{Zn} and Cu_{Zn} and charged Fe_{Zn} and Ni_{Zn} observed experimentally as electron paramagnetic resonant (EPR) centers.[5–8] They generally obey Hund's rules so that $S=5/2$, $3/2$, $3/2$, and $1/2$ for Fe^{3+}, Co^{2+}, Ni^{3+}, and Cu^{2+}, respectively. Admittance spectroscopy[9] indicates that Cu_{Zn} has an acceptor $(-/0)$ level 170 meV below E_c, the conduction-band minimum.

Optical transitions have been assigned to Cu^{3+} and Cu^{+},[10] although recent evidence suggests that transitions correlated with Cu may actually arise from vanadium.[11] Optical transitions are assigned[10,12] to $Co_{Zn}{}^{2+}$, $Fe_{Zn}{}^{3+}$, and several oxidation states of Ni_{Zn}. There is also EPR for $Fe_{Zn}{}^{3+}$ in material codoped with Li_{Zn} acceptors.[13] Since the $(-/0)$ level of Li_{Zn} is within 0.5 eV of the valence-band top (E_v),[14–17] the donor, $(0/+)$ level of Fe_{Zn} must be higher in the band gap.

Cobalt-doped ZnO is reported to be insulating,[18] particularly with high concentrations of Co.[19,20] It is also of interest for ferromagnetic semiconductor applications,[5,21,22] with electron diffraction showing little distortion to the ZnO matrix even for high concentrations of Co ($\sim$10%), the majority of Co substituting for Zn.[23] Theoretically, Co_{Zn} is a double donor, with levels close to E_v and around E_v +0.75 eV.[24]

The production of ZnO devices has been hindered by difficulties in fabricating *p*-type material. Recently, doping with pnictogens substituting for oxygen shows great promise,[25–32] but a key problem to be overcome to produce *p*-type ZnO is that as-grown material typically exhibits strong *n*-type conductivity. The nature of the donor responsible remains contentious. Interstitial hydrogen (H_i), a shallow donor,[33–35] is one possibility, but is not always the dominant donor.[36] Alternative candidates include native defects.[37] Indeed, the role of *isolated* H_i as a stable dopant is questionable since deuterium is known to readily diffuse in ZnO, with an activation barrier measured at just 170 meV.[38] Additionally, material indiffused with hydrogen initially shows a considerable increase in free electron concentration which is unstable at room temperature, consistent with relatively mobile hydrogen donors.[39] Since as-grown *n*-type conductivity persists in material annealed to 600 °C,[38] the donor(s) responsible must be more stable than the hydrogen-related donors created by indiffusion. Traps, such as lattice vacancies and impurities, will remove H_i donors from solution: impurity-hydrogen complexes are very stable with the presumably trap-limited activation barrier for the loss of hydrogen in Cu-doped material of 0.91 eV.[40] It is difficult to see how hydrogen alone can give rise to thermally stable conductivity. However, we shall show in this paper that thermally stable H-containing complexes also act as shallow donors.

Irrespective of the doping role of hydrogen, experimental observation of H-related centers indicates that it is a key impurity, which is unsurprising given its prevalence under typical growth conditions. Theoretically, isolated H_i forms a strong bond with oxygen, lying in either a bond-centered or an antibonding location. Both forms result in undercoordinated Zn displaced significantly from the host site.[33] In general, the structure of impurity-hydrogen complexes is less well understood. As TM impurities are also ubiquitous in as-grown crystals, the formation of metal-hydrogen complexes seems highly likely. Indeed, infrared- (IR-) absorption[40–43] and EPR (Ref. 44) studies indicate the formation of such complexes.

IR-absorption spectroscopy is a potent tool for chemically sensitive characterization, as the frequency of local vibrational modes (LVM's) is dependent on the mass, bonding, and local environment of the impurities. Various H-containing centers have been observed via IR[40–43,45–48] and Raman spectroscopy,[49] and agreement with theoretical modeling[33,41] has led to atomistic models in some cases.

(i) IR bands[45,47] at 3326.3 (2470.2) cm^{-1} have been linked to isolated, antibonded H_i (D_i).[41] Polarization indicates that the transition dipole is $\sim$110° to the *c* axis.[47]

(ii) H-I, located at 3611.3 (2668.0) cm^{-1} for H (D) is polarized along the *c* axis and has been correlated with H_i at a bond-centered location,[41,42] possibly associated with another defect not involved in the vibrations. Data from mixed H/D material indicates one H atom is involved.[41]

(iii) A band at 3577.3 cm^{-1} (H-I*) has been tentatively assigned to the O—H$\cdots$Ni complex,[42] and more recently

O—H···Li[48,50] aligned along the *c* axis, although there was no direct evidence for the presence of Ni or Li. The D mode is at 2644.4 cm^{-1}.[48]

(iv) A pair of IR bands labeled H-II (3349.6 and 3312.2 cm^{-1}), polarized approximately perpendicular and parallel to the *c* axis, respectively, are assigned to V_{Zn}—H_2 (V_{Zn} being the zinc-vacancy), where one O—H bond lies along the *c* axis. In material containing deuterium and mixed H/D isotopes the modes lie at 2486.3 and 2460.7 cm^{-1} ($V_{Zn}D_2$) and 3346.6, 3315.2, 2484.6, and 2463.0 cm^{-1} (V_{Zn}HD). The small shift with mixed H/D suggests weakly coupled vibrations.[41] The mixed isotopes data also show that the H atoms are inequivalent.

(v) Cu-I, located at 3191.8 (2378.9) cm^{-1} for H (D), is assigned to bond-centered hydrogen aligned perpendicular to the *c* axis.[40,43] This defect may also seen as an EPR center (labeled I in Ref. 51), although there is no evidence linking the two observations.[51] Sidebands in the IR spectrum of Cu-I are consistent with the presence of defects with multiple Cu/H components, giving rise to a complicated vibrational spectrum. A second band (Cu-II) at 3214 (2394) cm^{-1} is also present at 15 K and jumps to higher frequency above ~40 K.[40]

The thermal stability of the IR bands varies considerably: Cu-I, H-I, H-II, and H-I* anneal out around 650, 400, 550–600 °C and somewhere between 350 and 1200 °C, respectively. Additionally, the 3326.3 cm^{-1} band is lost with an activation energy of 1.2 eV.[42,45] Due to the very low activation barrier for isolated hydrogen,[38] any bands associated with H in noncryogenic material are most probably the result of *trapped* hydrogen.

As alluded to above, Cu—H centers are also detected via EPR,[44,51] with models proposed for three centers: Cu_{Zn}—$H_{BC_\perp}$ (spectrum I), Cu_{Zn}—Cu_i—H_i (spectrum II), and Cu_{Zn}—Cu_{Zn}—H_i (spectrum III). The presence of these centers depends on the concentration of Cu, with spectrum I being photosensitive, suggestive of a structural, electronic, or charge excitation, the latter of which is required to have a single unpaired electron. Due to the potential importance of TM impurities and TM-H complexes, we have calculated the structure, electrical levels, energetics, and vibrational modes of a range of complexes and their constituent species. In order to validate our method we have also simulated H_i and V_{Zn}—H_n, $n=1,2$, for comparison with previous theory and experiment.

II. METHOD

Local-spin-density-functional calculations were carried out using AIMPRO (*ab initio* modeling program) (Ref. 52) with periodic boundary conditions. We employ pseudopotentials,[53] with the valence wave functions described using a basis of sets of independent *s*, *p*, and *d* Gaussian orbitals with four different exponents sited at each atom site. Typically, a regular mesh of 2^3 **k** points is used to sample the band structure,[54] and the charge density is Fourier transformed using plane waves with an energy cutoff of 300 Ry. The Zn and O basis sets reproduce the lattice constants of wurtzite-ZnO (w-ZnO) to within 0.4%. The calculated band gap of 1.3 eV (which greatly underestimates the experimental direct band gap of around 3.4 eV) is in line with previously reports.[55,56]

Unless otherwise stated, results relate to a 96-atom orthorhombic supercell, with vectors $[3\bar{3}00]a$, $[22\bar{4}0]a$, and $[0002]c$ relative to the primitive w-ZnO lattice vectors. Some calculations used supercells containing 72 atoms (hexagonal, $[3000]a$, $[0300]a$, and $[0002]c$) or 144 atoms (orthorhombic, $[3\bar{3}00]a$, $[22\bar{4}0]a$, and $[0003]c$).

Formation energies are calculated using[57]

$$E^f(X^q) = E(X^q) - \sum_i \mu_i + q[E_v(X^q) + \mu_e] + \xi(X^q), \quad (1)$$

where $E(X^q)$ is the total energy for system X in charge state q, μ_i and μ_e are the chemical potentials of the atoms and electrons, and ξ is a correction for the periodic boundary conditions.[58] We approximate ξ by a Madelung term, $\sim 0.23q^2$eV for the 96-atom supercell.

In accordance with usual practice, we define μ_{Zn} over a range from Zn-rich (ZnO in equilibrium with Zn metal) to O-rich (ZnO in equilibrium with oxygen gas) conditions. μ_O is dependent on μ_{Zn}, and defined by $E(\mathrm{ZnO}) = \mu_O + \mu_{Zn}$, where E(ZnO) is the energy per bulk Zn—O pair. This yields a 3.7 eV range for μ_{Zn}, in agreement with previous

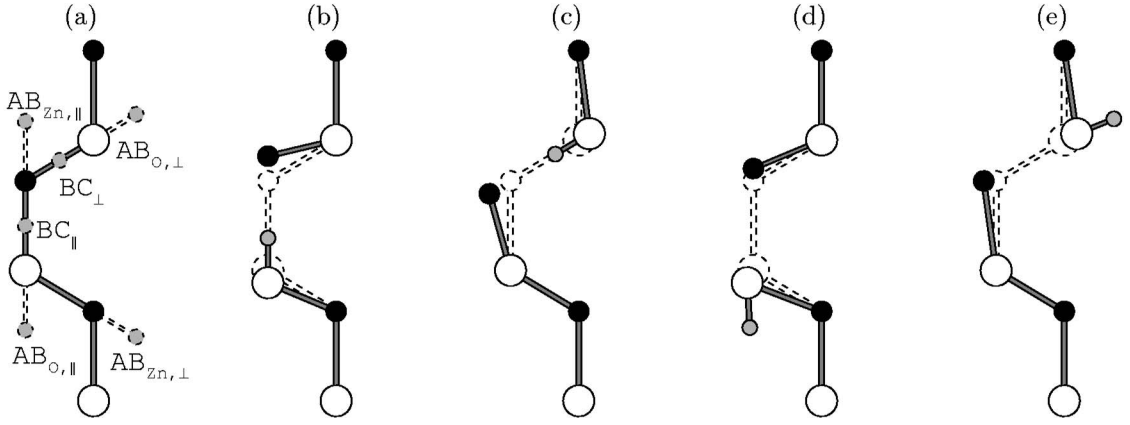

FIG. 1. (a) Schematic showing sites for H in ZnO. (b)–(e) show structures subsequent to relaxation with the ideal sites indicated by dashes. Black, white, and gray circles represent Zn, O, and H atoms, respectively. The vertical and horizontal axes are [0001] and $[2\bar{1}\bar{1}0]$.

theory[16,55] and experiment.[59] We define the quantity $\Delta\mu_{Zn} = E(\mathrm{Zn(hcp)})/2 - \mu_{Zn}$, so that $\Delta\mu_{Zn}$ has the range 0–3.7 eV, with $\Delta\mu_{Zn}=0$ corresponding to Zn-rich conditions. For other species we use H_2, fcc Cu and Ni, hcp Co, and bcc Fe.

Approximate electrical levels are obtained using Eq. (1). The underestimate of the band gap leads to some difficulty, and we therefore always review the calculated values in the context of the Kohn-Sham band structure. We estimate thermal stabilities using the calculated binding energies using the approximation that the rate of dissociation is given by

$$D = \omega_a \exp\{-E^a/k_B T\}, \tag{2}$$

where ω_a is the attempt frequency (taken to be approximately the defect vibrational frequency) and E^a is the activation energy, which may be taken as a first approximation to be the sum of the binding energy[60] and the barrier to migration of the more mobile component. As binding energies are calculated from formation energies,[60] this implicitly includes a correction for the the periodic boundary condition. Note the errors due to the underestimation of the band gap and the proximity of impurity $3d$ states to the conduction-band impact on the formation energies and hence the binding energies. For D, the order of unity, $T \sim E^a/k_B \ln \omega_a$. Given the crudeness of the model, the thermal stability thus inferred is only semiquantitative in nature.

Finally, vibrational modes are calculated by obtaining second derivatives of the energy with respect to the atom positions for the defect atoms and their immediate neighbors. The dynamical matrix is then made up from a combination of these terms with others obtained from a valence-force potential fitted to *ab initio* bulk force constants for the remaining host atoms in the supercells. A full description of the method used is given in Ref. 52. The use of the valence-force potential has a negligible affect on high-frequency modes, but is important in the estimation of defect modes resonant with the one-phonon bands. *X*-H stretch modes arise from highly anharmonic vibrational potentials, so the calculated, quasiharmonic stretch-mode frequencies listed in this study are therefore likely to be in error due to the neglect of this anharmonicity by an amount of the order of 100 cm^{-1}.[41,61,62] Finally, the orthorhombic supercells do not allow for threefold rotational axes, so that trigonal systems are reduced to C_s symmetry. This artificially splits degenerate modes, typically by a few wave numbers, so where appropriate we quote the average value of these degenerate pairs.

III. RESULTS

In order to validate the method, we first present the properties of isolated H_i, the hydrogen molecule, and V_{Zn}—H_n complexes in Secs. III A–III C. In the remaining sections we present the results for substitutional and interstitial TM's along with Cu pairs (Sec. III D), followed by a range of TM–H complexes (Sec. III E).

A. Interstitial hydrogen

We examined the locations for H_i shown schematically in Fig. 1(a). All relaxed structures result in undercoordinated

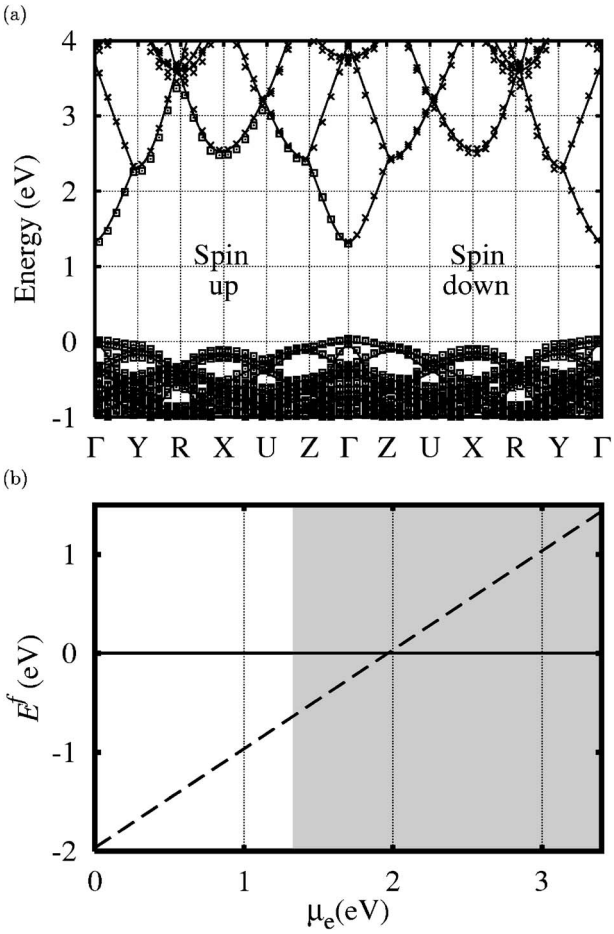

FIG. 2. (a) The band structure for $H_{BC_\parallel}$. Occupied (empty) bands are shown as squares (crosses), with lines indicating the bands of a defect-free supercell. The zero of energy is set at E_v of bulk ZnO. Special k points are indicated using the notation of Koster (Ref. 65) (b) E^f for neutral (solid line) and positively charged (dashed line) $H_{BC_\parallel}$. The shaded region indicates the theoretical to experimental band-gap range.

Zn. In particular, with bond-centered hydrogen, Zn relaxes to be approximately coplanar with three O neighbors [Figs. 1(b) and 1(c)], representing 4% shorter Zn—O bonds. This qualitatively agrees with previous calculations.[33,63,64] $H_{AB_{Zn}}$ are unstable, relaxing to H bonded to oxygen. We also examined $H_{BC_\parallel}$ and $H_{AB_{O,\parallel}}$ in 72- and 144-host-atom supercells, with the resultant structures being indistinguishable from those for 96-atom supercells.

The different sites are very similar in energy, the lowest-energy structure being $H_{BC_\parallel}$, with the others being up to 0.3 eV higher (Table V). This agrees with recent theory[63] and differs from Van de Walle.[33] The ordering of the energies of the different sites is independent of cell size in our calculations.

All structures show similar electronic structures: Figure 2(a) shows the band structure of $H_{BC_\parallel}$. The formation energy of H_i [Eq. (1)], shown in Fig. 2(b), yields a (0/+) level around E_v+2 eV. This is above the theoretical value for E_c, but within the experimental band gap, leading to some questions over interpretation. However, combining the formation-

TABLE I. LVM frequencies (irreducible representations) for H and D in the structures shown in Figs. 1(b)–1(e) (cm^{-1}). The bend modes of $D_{BC_\parallel}$ drop below the one-phonon maximum.

		Hydrogen		Deuterium	
Structure	Sym	Bend	Stretch	Bend	Stretch
$H_{BC_\parallel}$	C_{3v}	646(E)	3620(A_1)	—	2632(A_1)
		722(A'')			
$H_{BC_\perp}$	C_s	938(A'')	3387(A')	687(A'')	2467(A')
$H_{AB_{O,\parallel}}$	C_{3v}	1013(E)	3288(A_1)	842(E)	2394(A_1)
		929(A')		748(A')	
$H_{AB_{O,\perp}}$	C_s	1020(A'')	3252(A')	844(A'')	2370(A')

energy and band-structure data strongly suggests that neutral H_i can be described as H_i^+ with an electron in the conduction band. This interpretation is in line with previous theoretical studies.[33,66–68]

We now turn to the LVM's. Each structure gives rise to bend and stretch modes, which are summarized in Table I. As found previously,[41] H_{AB_O} gives rise to a lower-frequency stretch mode relative to H_{BC}, but higher-frequency bend modes.

An assignment[47] of the 3326.3-cm^{-1} band to isolated H_{AB_O} is superficially at odds with the total energies indicating H_{BC} to be most stable. However, the total energies are similar (Table V), and inclusion of zero-point energies reduces the differences between H_{BC} and H_{AB_O}, so the latter cannot be ruled out on energy grounds.

More significant is that deuterium migrates with an activation energy of just 170 meV,[38] comparable with the zero-point energy. From preliminary calculations, our estimate of a migration barrier for hydrogen ($H_{BC} \rightarrow H_{AB_O} \rightarrow H_{BC} \cdots$) using standard constrained relaxations indicates a barrier around 0.2 eV, comparable to the experimental value, supporting the association of the 170-meV barrier with free migration of D in bulk ZnO. Since the 3326.3-cm^{-1} band is lost with an activation energy of 1.2 eV,[45] it seems unlikely that the 3326.3-cm^{-1} band can be attributed to *isolated* H_i. Since the stress response of the 3326.3-cm^{-1} band indicates H_{AB_O},[63] it is plausible that it originates from H_{AB_O} trapped at a defect and bound by ~1 eV.

B. Hydrogen molecules

A molecule relaxed at a cage site was found to be preferentially aligned along the c axis with a bond length of 0.77 Å, close to that calculated for free hydrogen using our computational framework. The defect structure is in close agreement with previous calculations,[33] but in contrast we find that H_2 has practically the same energy as two isolated H_i. If one were to consider the dissociation of the molecule into two separated H_i^+ and two e^-, then the chemical potential of the electrons must be taken into account. In hydrogen-rich material μ_e will be close to E_c and the neutral reaction detailed above applies. For μ_e lower in the gap the energy released in the dissociation reaction is increased by up to twice the band-gap energy, making the reaction even more favorable.

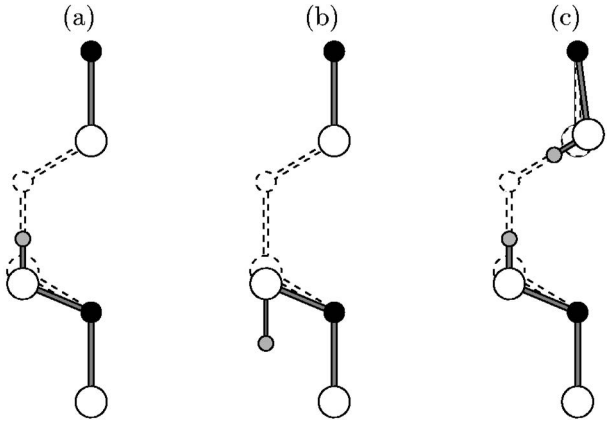

FIG. 3. Schematics of V_{Zn} with (a) internal hydrogen aligned along c, (b) antibonded hydrogen aligned along c, and (c) V_{Zn}—H_2. The shading and axes are as defined in Fig. 1.

We calculate that the molecule has a stretch mode around 4032 cm^{-1}, with HD and D_2 species having modes at around 3497 and 2852 cm^{-1}, respectively. As a reference, the free molecule has a calculated stretch mode of 4157 cm^{-1}, suggesting that H_2 in ZnO would have a vibrational frequency close to the free molecule value.

C. Vacancy-hydrogen complexes

We find V_{Zn} results in a small contraction of the surrounding lattice, with neighboring Zn—O bonds shortened by ~2%. As previously reported,[55] we find that V_{Zn} is a double acceptor, with (−/0) and (2−/−) levels at E_v+0.1 eV and E_v+1.2 eV, respectively. The formation energy (and hence equilibrium concentration) is dependent on the growth environment via $\Delta\mu_{Zn}$ (Sec. II) so that $E^f(V_{Zn})$ ranges from 3.7 to 7.4 eV for V_{Zn}^0. However, in n-type material, V_{Zn} will be negatively charged so that in the oxygen-rich limit with $\mu_e \sim E_c$, $E^f(V_{Zn}^{2-})$ may be small or negative and V_{Zn} may then be expected to form in large concentrations.

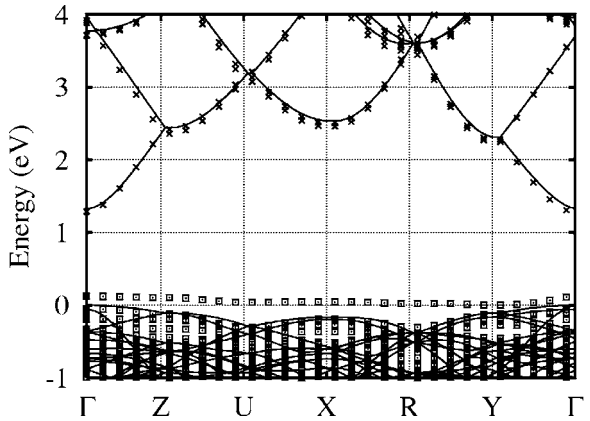

FIG. 4. The Kohn-Sham band structure for V_{Zn}—H_2. Symbols and axes are as in Fig. 2.

TABLE II. LVM's for V_{Zn}—H_n structures (cm^{-1}) and their symmetries. For the mixed isotope case, the first species refers to that contained in a O—H bond aligned approximately parallel to the c axis. All modes are IR and Raman active by symmetry.

			Hydrogen			Deuterium		
Structure	Sym		Bend		Stretch	Bend		Stretch
V_{Zn}—$H_{\parallel}$	C_{3v}		877(E)		3255(A_1)	660(E)		2372(A_1)
V_{Zn}—$H_{\perp}$	C_s		832(A'')	856(A')	3272(A')	636(A'')	647(A')	2384(A')
V_{Zn}—$H_{AB_{O,\parallel}}$	C_{3v}		892(E)		3554(A_1)	665(E)		2580(A_1)
			684(A'')	803(A'')	3228(A')	—	—	—
		HH	928(A')	1097(A')	3267(A')	—	—	—
		HD	774(A'')	1026(A')	3247(A')	599(A'')	719(A')	2367(A')
V_{Zn}—H_2	C_s	DH	738(A'')	1033(A')	3249(A')	604(A'')	722(A')	2365(A')
			—	—	—	591(A'')	633(A'')	2354(A')
		DD	—	—	—	684(A')	794(A')	2379(A')

Various configurations of V_{Zn}—H were studied, the position of hydrogen corresponding to the sites indicated in Fig. 1(a). We find that V_{Zn}—H is energetically most favorable with H lying along the c axis [Fig. 3(a)], with the off-axis structure being just 25 meV higher in energy. Structures with H_{AB_O} [Fig. 3(b)] are all ~1 eV higher in energy than when H is "inside" the vacancy. V_{Zn}—H is partially passivated, with a (−/0) level at E_v+0.46 eV. H_i^+ is bound to V_{Zn}^- and V_{Zn}^{2-} by 2.4 and 3.2 eV, respectively, suggesting it would be stable up to around 900–1200 K, provided it does not migrate as a complex.

As found previously[41] and consistent with the polarization and inequivalence of the H atoms in the H-II IR bands, we find that the structure in Fig. 3(c) is marginally the lowest-energy form of V_{Zn}—H_2: the structure without an O—H bond along the c axis is only around 20 meV higher in energy. Note that both types of V_{Zn}—H_2 give rise to LVM's polarized in line with H-II, and it is therefore on the basis of the polarization *and* inequivalence of the H atoms that an assignment of H-II to Fig. 3(c) can be made. The addition of two hydrogen atoms to V_{Zn} completely passivates it, yielding only a filled defect band close to the valence-band top (Fig. 4). This is in line with previous theory.[41] Mulliken analysis indicates that the defect band is highly localized and associated with p orbitals on the unhydrogenated O atoms at the vacancy.

The saturation of the vacancy with hydrogen is highly energetically favorable: $V_{Zn}^{2-}+2H_i^+ \rightarrow V_{Zn}$—$H_2$ liberates 5.4 eV. Our estimate is substantially greater than that reported previously[41] and greater than the 2.2 eV suggested using Eq. (2) and the experimental annealing temperature of H-II of 550 °C. However, $(V_{Zn}$—$H)^- + H_i^+ \rightarrow V_{Zn}$—$H_2$ liberates just 2.2 eV, indicating that this is the rate limiting step in the annealing of H-II. Indeed, since V_{Zn}—H_2 binds the second H more weakly than the first, thermodynamically V_{Zn}—H_2 would be expected to occur in large concentrations only where $[H_i]$ exceeds $[V_{Zn}]$. The agreement between the binding energy of the second H atom gives us some confidence in comparing these calculated values with experiment in other cases.

Table II lists the LVM's for $V_{Zn}H_n$. The frequencies and polarization are in good agreement with the observed H-II modes.[41] In particular, the calculated splittings of 39 and 25 cm^{-1} for H and D are in excellent agreement with the experimental values of 37.4 and 25.6 cm^{-1}, as is the V_{Zn}—H_2/V_{Zn}—D_2 isotope shift.

Complexes with three and four hydrogen atoms were also examined. Although additional H formed bonds with O atoms, they simultaneously donate electrons to the conduction band, rendering V_{Zn}—H_3 and V_{Zn}—H_4 shallow donor and double-donor systems, respectively. Furthermore, it *costs* energy to put additional H_i into V_{Zn}—H_2, suggesting such defects would not form.

TABLE III. Key calculated parameters for TM_{Zn} in ZnO. The changes in nearest-neighbor (NN) bond lengths are relative to Zn—O distances, with the change in axial bond length given first. Electrical levels are relative to E_v (eV). Formation energies are calculated with $\Delta\mu_{Zn}=0$ and μ_e at E_v.

	$(TM_{Zn})^+$			$(TM_{Zn})^0$			$(TM_{Zn})^-$				
TM	S	E^f	NN	S	E^f	NN	S	E^f	NN	(0/+)	(−/0)
Cu	1	2.6	−3%, −2%	1/2	2.9	−1%, −1%	0	4.9	0, +1%	0.3	2.0
Ni	3/2	2.0	−4%, −4%	1	3.0	−1%, −1%	1/2	5.4	0, 0	1.1	2.4
Co	2	1.5	−6%, −6%	3/2	1.8	−4%, −4%	2	3.7	−4%, −4%	0.3	1.9
Fe	5/2	−2.2	−6%, −5%	2	−0.1	−6%, −5%	5/2	2.0	−4%, −4%	2.1	2.2

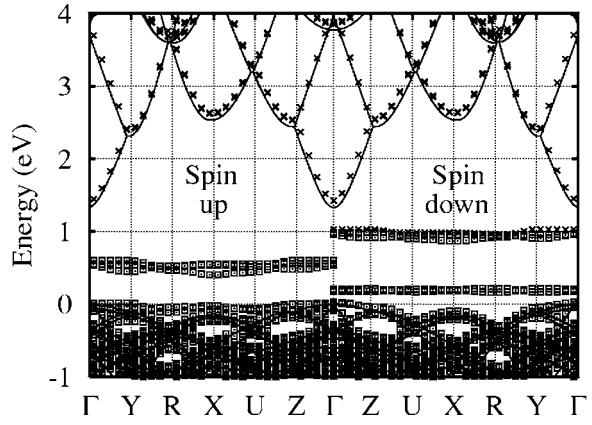

FIG. 5. The Kohn-Sham band structure for Cu_{Zn}. Symbols and axes are as in Fig. 2.

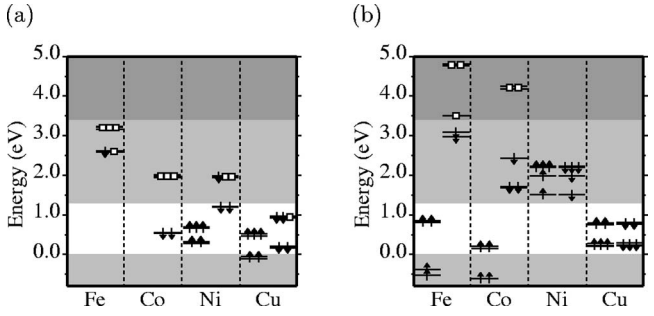

FIG. 6. $3d$ impurity bands for TM centers in ZnO. (a) TM_{Zn} and (b) TM_i. The light- and dark-gray regions indicate the theoretical and experimental band gaps, respectively. The missing spin-up $3d$ bands for Fe and Co lie deeper in the valence band. An additional, non-$3d$ electron lies in the conduction band for Fe_i, Co_i, and Cu_i.

D. Transition metals: Fe, Co, Ni, and Cu

1. Substitutional TM's: TM_{Zn}

TM_{Zn} are tensile, increasingly so with decreasing atomic number Z (Table III). Hund's rule dictates that S increases with decreasing Z, which is what we find in our calculations (Table III). In particular, we reproduce the ground-state spins of Fe^{3+}, Co^{2+}, Ni^{3+}, and Cu^{2+} as determined from EPR.[5–8] For example, the $S=1/2$ and $S=5/2$ of Ni^{3+} lie, respectively, 0.5 eV and 2.3 eV higher energy than the $S=3/2$ ground state. This gives us some confidence in the calculated spin states for other species.

$E^f(TM_{Zn})$ is lowest in Zn-lean material, showing a trend with Z (Table III). Given the inaccuracies in the method and somewhat arbitrary nature of μ_{TM}, the formation energies are only a guide, but indicate that in Zn-lean growth conditions one would expect a large concentration of substitutional TM impurities. This result is in line with the large concentrations of Co that can be attained while retaining the basic ZnO structure.[23,69,70]

The $(-/0)$ level of Cu_{Zn}, measured at E_c-170 meV,[9] can be understood from a combination of the band structure (Fig. 5) and the $(-/0)$ level calculated to lie close to the $(0/+)$ level of H_i. We conclude that theory is consistent with the assignment of a $(-/0)$ level close to the conduction band,[9] but this highlights the difficulty in interpreting the calculations. Equation (1) also yields a donor for Cu_{Zn} close to the valence-band top.

The electronic picture becomes increasingly complicated as the $3d$ bands rise in energy relative to E_v with decreasing Z. For Fe_{Zn}, Co_{Zn}, and Ni_{Zn} the impurity $3d$ bands cross the host conduction bands at the Brillouin-zone center, as illustrated in Fig. 6. The high energy of the $3d$ bands is in line with other calculations where the band-gap problem is somewhat reduced,[71] and we therefore expect the results presented here to be qualitatively correct. Equation (1) yields $(-/0)$ levels above the theoretical conduction-band minimum (Table III), but as seen with Cu_{Zn}, this does not rule out acceptor activity. However, the location of the $3d$ bands for these systems is higher in energy than Cu_{Zn} (Fig. 6) and it is not possible to be conclusive; the band structures for Ni, Co, and Fe suggest that the added electron in the negative-charge state may be more associated with the conduction band than the states of the metal. No centers have $(2-/-)$ levels.

The $(0/+)$ levels of Ni_{Zn} and Fe_{Zn} lie relatively high in energy, above or around the theoretical value for E_c. This is consistent with the observation of the ionized impurities via EPR. In both cases the band structure (not shown) indicates that there is an electron in the conduction band at least for some values of k around the Γ point. However, at the R point, where the theoretical band gap is largest, $3d$ bands lie in the band gap (Fig. 6). We conclude that Fe_{Zn} and Ni_{Zn} may contribute to n-type conductivity in as-grown material. Our estimate for the $(0/+)$ level of Co_{Zn} is much lower in the band gap than previously predicted,[24] and we find no second donor level in the band gap. We find that the Γ-point approximation *lowers* the donor level by around 0.3 eV and cannot account for the different levels. It seems more probable that either the way E_F is calculated for the formation energy[24] of charged systems or the use of different spin states (which were not disclosed in Ref. 24) is responsible for the discrepancy. Since we find that electrical levels have meaning only when viewed in tandem with band structures, the differences are not critical.

2. Interstitial TM's: TM_i

We examined bond-centered (described in Sec. III A), octahedral (O), and tetrahedral (T) interstitial sites.[72] The bond-centered site was unstable. The relaxed structures for Cu_i at the O and T sites are shown as representative examples in Fig. 7. The O site was most stable for Fe_i, Co_i, Cu_i, and Zn_i, with the T site being favored by Ni_i (Table IV). The structure of Cu_i shown in Fig. 7(c), denoted T, is distorted from the ideal axial symmetry. This symmetry reduction, seen for all TM's, lowers the total energy by 0.5–3 eV, depending on the TM, and is particularly large for Ni.

The band structure of Cu_i (Fig. 8) is very similar to that of H_i, with an electron in the conduction band and a $(0/+)$ level lying around $E_v+2.0$ eV. The $3d$ bands of Cu lie in the band gap, split into a triplet and a doublet by the crystal field. The general picture is similar for the other TM dopants (Table IV and Fig. 6), with the $(0/+)$ level related to the $3d$ bands lying in the upper part of the band gap.

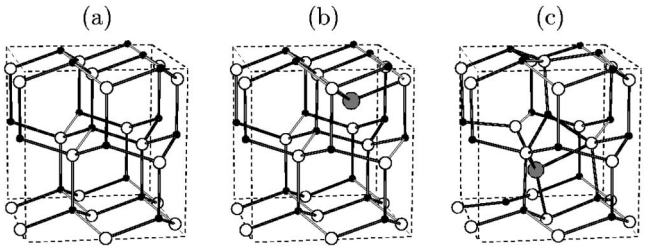

FIG. 7. The relaxed geometries for Cu_i at the (b) *O* and (c) *T* cages sites. (a) shows a section of defect-free w-ZnO for comparison. Black, white, and gray circles represent Zn, O, and Cu, respectively. The vertical indicated by the dashed boxes are aligned along the *c* axis, with the horizontal and normal directions $[2\bar{1}\bar{1}0]$ and $[01\bar{1}0]$, respectively.

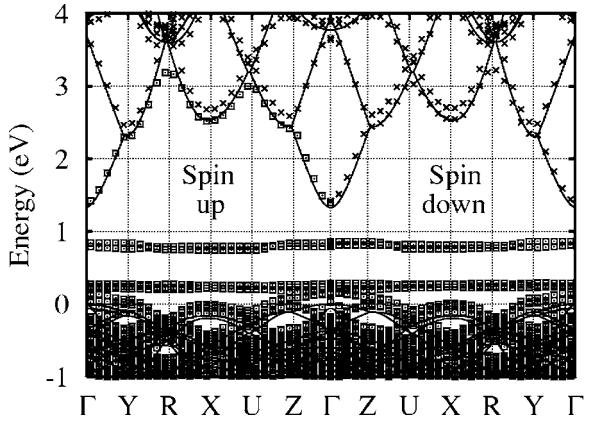

FIG. 8. The Kohn-Sham band structure for Cu_i. Symbols and axes are as in Fig. 2.

The effective spins of the TM_i defects deviate from Hund's rule where they represent autoionizing centers (Co_i and Fe_i). For instance, the band-structure evidence suggests that neutral Fe_i should be regarded as $(Fe_i)^+(\uparrow\uparrow\uparrow)+e^-(\uparrow)$. However, these differ in energy from the spin indicated by Hund's rule by a small amount. Indeed, all of the TM_i we have examined appear to be shallow donors.

$E^f(TM_i)$ (Table IV) are independent of $\Delta\mu_{Zn}$ and considerably higher than the corresponding TM_{Zn}. However, in *p*-type material they are will be positively charged and have a greatly enhanced solubility.

3. Trends in formation energies

The concentrations of different forms of TM in ZnO are driven by their formation energy, and therefore dependent on $\Delta\mu_{Zn}$, μ_{TM}, and μ_e. The choice of μ_{TM} is not unique, but is best chosen to reflect the appropriate states from which the atoms are taken. Taking into account the stable charge states, the defect with the lowest formation energy for a given $\Delta\mu_{Zn}$ and μ_e can be determined.

Figure 9 shows the ranges of $\Delta\mu_{Zn}$ and μ_e for which different configurations and charge states are calculated to have the lowest formation energy. For example, Fig. 9(a) includes the dark gray region towards lower $\Delta\mu_{Zn}$ (Zn-rich) and *p*-type material corresponding to conditions favoring Cu_i incorporation. The underestimate in the band gap and the uncertainty in the electrical levels leads to uncertainty in the appropriate range for μ_e. However, the electronic parts of the calculations are mutually consistent and are therefore expected to yield qualitatively significant results.

Some general conclusions can be drawn. Large areas of stability exist for charged substitutional and interstitial defects, with the area of stability for the Hubbard *U* value reducing as *Z* decreases. TM_{Zn} are most stable in the Zn-lean regime. TM_i forms mostly in *p*-type, Zn-rich material and is more likely to form for higher *Z*.

E. Transition-metal hydrogen complexes

1. TM_{Zn}—H_i

TM_{Zn}—H_i complexes were studied using the six H_i sites shown in Fig. 1(a). In all cases the ground state was TM_{Zn}—H_{BC}, with the TM_{Zn}—$H_{BC_\parallel}$ and TM_{Zn}—$H_{BC_\perp}$ being very close in energy. TM_{Zn}—$H_{AB_{TM}}$ structures are increasingly stable for lower *Z*, dependent on the effective spin. In particular, Fe_{Zn}—$H_{AB_{Fe}}$ is metastable for $S=1/2$, but unstable for $S=5/2$, the ground state for Fe_{Zn}—H_{BC}. The energies are summarized in Table V. The effective spins are the same as negatively charged TM_{Zn}. All TM_{Zn}—H_i complexes have (0/+) levels (Table V), but in all cases except Cu_{Zn_2}, the band structures indicate that, at least in the vicinity of the Γ point, there is an electron at or above the theoretical conduction-band minimum. The centers therefore represent H-related donors with a much greater thermal stability than isolated H_i.

TABLE IV. TM_i formation energies ($\Delta\mu_{Zn}=0$, μ_e at E_v), the relative energies of the *T* and *O* sites ($\Delta E^{T\text{-}O}$), the ground-state effective spin (*S*) for the neutral-charge state, and the electrical levels of relative to E_v, calculated from Eq. (1). ΔE^{S-1} and ΔE^{S+1} indicate the relative energies of higher and lower effective spins. All energies in eV.

TM	E^f	$\Delta E^{T\text{-}O}$	*S*	ΔE^{S-1}	ΔE^{S+1}	(−/0)	(0/+)	(+/2+)
Zn	1.7	0.6	0	—	1.8	—	1.9	1.4
Cu	2.3	0.3	1/2	—	2.7	2.6	2.0	—
Ni	3.1	−0.3	0	—	0.1	2.6	2.0	1.1
Co	2.8	0.5	3/2	0.4	1.4	—	1.6	0.4
Fe	1.9	0.8	2	0.8	0.9	—	1.7	1.5

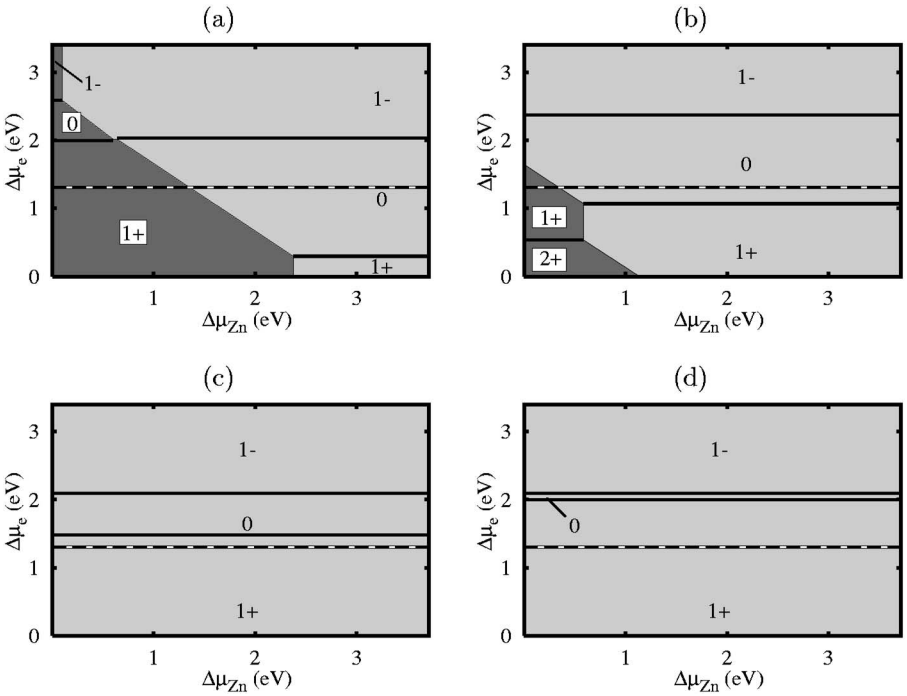

FIG. 9. Plot of the regions of minimum E^f for monomer defects of (a) Cu, (b) Ni, (c) Co, and (d) Fe in w-ZnO as a function of μ_{Zn} and μ_e. The dashed horizontal line indicates the theoretical band gap. The light region represents TM_{Zn} and the dark TM. Horizontal lines represent electrical levels.

The binding energy has been estimated with respect to the relevant charged species (Table VI). There is generally a trend to more strongly bound complexes with higher Z. We can approximate the activation energy for dissociation to be E^b plus the hydrogen migration barrier, which we can take to be around 0.2 eV.[38] Thus an estimate of the thermal stability can be made using the method outlined in Sec. II. This yields a wide range of projected thermal stabilities, with Co_{Zn}—H_i being relative unstable and Cu_{Zn}—H_i likely to dissociate above 500 °C.

Park and Chadi[64] also find that H lies in a bond center for Co_{Zn}—H_i and report a binding energy of 0.83 eV, somewhat larger than the value we have found. However, their calculations used smaller supercells and a single Brillouin-zone sampling point which is likely to affect the binding energy. Indeed we have calculated a binding energy of 0.7 eV using the single **k** point at $(1/2,1/2,1/2)$, indicating that this choice of sampling can significantly affect binding and, indeed, formation energies and calculated electrical levels.

Since there are no TM—H bonds in the ground-state structures, the LVM's of the TM_{Zn}—H_i complexes (Table VII) are only indirectly dependent on the TM species, but may aid in the identification of the defect. By symmetry, all the modes in Table VII are IR and Raman active. The stretch mode for H_i approximately perpendicular to the c axis is higher in frequency than the on-axis configuration. There is no discernible isotopic shift with TM to the H modes, with calculated shifts significantly less than 1 cm^{-1}. The isotopic shift for O (Ref. 18) is found to be −10 and −13 cm^{-1} for O—H and O—D stretch modes, respectively, in excellent agreement with the shift observed by Gärtner.[40,43]

It is useful at this point to reflect on our results in the context of the Cu-I IR band and related EPR. First, the calculated stability for Cu—H complexes is qualitatively in line with the relative high annealing temperatures of the Cu-I IR band at 650 °C.[42] Additionally, the angle that the O—H bond makes with the c axis in Cu_{Zn}—$H_{BC_\perp}$ is 112°, in broad agreement with the 116° obtained from Fourier-transform (FT) IR studies.[44] However, neutral Cu_{Zn}—$H_{BC_\perp}$ cannot be responsible for the EPR center reported by Zwingel *et al.* The photosensitivity of the EPR center and the excitation energy of 2.05 eV obtained from experiment[51] are consistent with the ionization of Cu_{Zn}—H_i [the calculated (0/+) level is at E_v+0.8 eV], and the angle of 112° for the positive-charge state is in agreement with the 111° from the EPR data.[51] The charged complex has an O—H bond length

TABLE V. Total energy (eV) relative to the most stable structure for the various configurations of Tm_{Zn}—H_i shown in Fig. 1(a) and the ground-state effective spin. Dashes indicate forms that are unstable. The (0/+) levels (eV) are relative to E_v.

TM	$BC_\parallel$	$BC_\perp$	$AB_{O,\parallel}$	$AB_{O,\perp}$	$AB_{TM,\parallel}$	$AB_{TM,\perp}$	S	(0/+)
Zn	0.0	0.2	0.2	0.2	—	—	1/2	2.0
Cu	0.1	0.0	1.1	0.9	—	1.5	0	0.8
Ni	0.0	0.0	0.7	0.5	1.0	0.9	1/2	0.9
Co	0.0	0.3	0.3	0.4	1.8	1.5	2	1.4
Fe	0.0	0.0	0.5	0.8	—	—	5/2	1.7

TABLE VI. Energy required for dissociation reactions (eV). Those reactions that represent the energetically favorable dissociation path are indicated by boldface.

Reaction			V_{Zn}	Cu	Ni	Co	Fe
X—H	→	$X^-+H_i^+$	**2.4**	**1.9**	1.5	**0.5**	0.7
X—H	→	$X+H_i$	4.2	**1.9**	**1.1**	**0.5**	**0.4**
X—H_2	→	X—$H^-+H_i^+$	**2.2**	1.6	1.9	0.9	0.6
X—H_2	→	X—$H+H_i$	3.7	**0.9**	**1.1**	**0.3**	**−0.1**
X—H_2	→	$X+2H_i$	7.9	2.8	2.2	0.8	0.3

2% shorter than the neutral and concomitantly higher-frequency LVM's (Table VII), which are not in agreement with experiment. The upward shift in frequency with ionization is consistent with the thermally populated Cu-II IR center, but the calculated shift in frequency is an order of magnitude larger than the Cu-I/Cu-II splitting. An alternative interpretation of the Cu-II system is the thermal population of a different conformer of the same constituents, consistent with the calculated relative energies (Table V). However, we cannot be conclusive as to which, if either, of these processes can be attributed to the presence of the Cu-II IR bands.

Finally, there are no vibrational modes associated with Ni (or any other TM) that agree particularly with the H-I* bands, and we view such an assignment[42] as unlikely. We shall return to this in Sec. IV.

2. TM_{Zn}—H_n *complexes,* $n>1$

In line with Au—H complexes in Si,[73,74] it is likely that TM's can bind more than one H atom. We have studied various TM_{Zn}—H_2 structures constructed from $TM_{Zn}+2H_i$ and find that the most stable configurations have H lying in bond centers, one aligned along the c axis, and the other almost perpendicular (TM_{Zn}—$H_{BC_\parallel}$—$H_{BC_\perp}$) similar to V_{Zn}—H_2.

The effective-spin states of $S=1/2$, $3/2$, and 2, for Cu_{Zn}—H_2, Co_{Zn}—H_2, and Fe_{Zn}—H_2, respectively, should give rise to highly characteristic EPR spectra. Ni_{Zn}—H_2 is diamagnetic. In the case of Fe_{Zn}—H_2 the Kohn-Sham spectrum is consistent with the center autoionizing, so the Fe_{Zn}—H_2 ($S=2$) can be viewed as a parallel pair $(Fe_{Zn}—H_2)^+ + e^-$, where the additional electron is in the conduction band.

The second hydrogen in each complex is always less strongly bound than the first (Table VI), and, as with TM_{Zn}—H_i, H to be more strongly bound to a TM with higher Z.

The dihydride complexes (other than Cu) have an electronic structure similar to the TM two places to the right on the periodic table, but all systems examined have filled bands at or above E_c. In particular, Cu_{Zn}—H_2 strongly resembles the band structure of H_i and, being bound by 0.9 eV, represents a H-related shallow donor that may survive up to around room temperature.

The LVM's of the low-energy structures for all four TM_{Zn}—H_2 complexes are listed in Table VIII. There is an agreement between modes of Cu_{Zn}—H_2 and Cu—I for both H and D. However, the isotopic data show that Cu—I contains a single H atom, but Cu_{Zn}—H_2 might give rise to some of the complex array of sidebands. Yet Cu_{Zn}—H_2 is likely to be the dominant center in Cu-doped material where the concentration of H exceeds that of Cu (which was not the case in Zwingel's experiments[51]) and should be clearly identifiable from the LVM's and EPR spectrum.

A third H in all TM_{Zn}—H_3 is unbound and, as such, defects with more than two hydrogen are not expected to form in equilibrium conditions.

3. Cu_n—H_m *complexes*

Several specific models for IR and EPR centers have been proposed in the literature.

The side bands to the Cu-I IR center are proposed to be due to various conformers of nearest-neighbor Cu_{Zn} pairs trapping one or more H_i.[40,43] We will show elsewhere that TM_{Zn_2} centers are bound and able to trap hydrogen.[75] In particular, using the computational scheme presented above we find that Cu_{Zn_2} form antiferromagnetic pairs bound by 0.3 eV, which traps H_i in a bond-centered location bound by around 1.7 eV. We find that the lowest-energy structure places H_i along the c axis neighboring one of the Cu_{Zn}, but the relative energies of the other H_{BC} sites means that we

TABLE VII. The LVM's of the TM_{Zn}-H_i complexes in the neutral charge state (cm^{-1}).

		Hydrogen		Deuterium		
Structure	Sym	Bend	Stretch	Bend	Stretch	TM
Cu_{Zn}—$H_{BC_\parallel}$	C_{3v}	825(E)	2948(A_1)	624(E)	2145(A_1)	127(A_1)
Cu_{Zn}—$H_{BC_\perp}$		768(A'') 846(A')	3087(A')	604(A'') 629(A')	2246(A')	
Cu_{Zn}—$H_{BC_\perp}^+$	C_s	708(A'') 720(A')	3365(A')	654(A'') 658(A')	2448(A')	99(A'')
Cu_{Zn}—$H_{AB_{O,\parallel}}$	C_{3v}	851(E)	3416(A_1)	619(E)	2481(A_1)	42(A_1)
Ni_{Zn}—$H_{BC_\parallel}$	C_{3v}	859(E)	2744(A_1)	636(E)	1996(A_1)	35(A'') 171(A'')
Ni_{Zn}—$H_{BC_\perp}$	C_s	804(A'') 835(A')	2845(A')	612(A'') 624(A')	2070(A')	41(A'')
Co_{Zn}—$H_{BC_\parallel}$	C_{3v}	850(E)	2811(A_1)	630(E)	2045(A_1)	131(A_1) 166(A_1)
Co_{Zn}—$H_{BC_\perp}$	C_s	678(A'') 728(A')	3384(A')	666(A'') 682(A')	2463(A')	288(E)
Fe_{Zn}—$H_{BC_\parallel}$	C_{3v}	816(E)	2972(A_1)	642(E)	2162(A_1)	195(A_1) 289(E)
Fe_{Zn}—$H_{BC_\perp}$	C_s	742(A'') 782(A')	3100(A')	645(A'') 651(A')	2255(A')	197(A') 289($A'+A''$)

TABLE VIII. The LVM's of the TM_{Zn}—H_2 complexes in the neutral-charge state. All bend modes can be categorized as A'' modes, while stretch modes are A' (cm^{-1}).

		Hydrogen			Deuterium			
Structure		Bend		Stretch	Bend		Stretch	TM
Cu_{Zn}—H_2		784	790	3150	—	—	—	141
	HH	839	912	3195	—	—	—	162
	HD	831	865	3160	698	753	2319	
	DH	797	857	3186	697	753	2299	
		—	—	—	627	666	2294	
	DD	—	—	—	699	753	2325	
Ni_{Zn}—H_2		894	907	2528	—	—	—	142
	HH	934	973	2548	—	—	—	177
	HD	926	932	2541	698	730	1849	
	DH	909	948	2535	697	730	1852	
		—	—	—	682	695	1845	
	DD	—	—	—	709	730	1856	
Co_{Zn}—H_2		741	772	3162	—	—	—	141
	HH	788	833	3176	—	—	—	161
	HD	780	816	3168	—	—	2308	
	DH	765	811	3169	—	—	2307	
		—	—	—	—	—	2302	
	DD	—	—	—	692	802	2312	
Fe_{Zn}—H_2		685	790	2932	—	—	—	93
	HH	839	850	3067	—	—	—	287
	HD	839	850	3067	—	602	2135	
	DH	685	790	2932	620	625	2232	
		—	—	—	—	602	2135	
	DD	—	—	—	620	625	2232	

cannot rule out the site proposed by Zwingel[51] for the spectrum-III center. The calculated vibrational modes are close to those of Cu_{Zn}—H_i.

Cu_{Zn}—Cu_{Zn}—H_i strongly binds a second H_i, rendering it diamagnetic, but the various conformers give rise to a wide range of vibrational modes. For example, where $Cu_{Zn,2}$—H_2 is made up from parallel Cu_{Zn}—$H_{BC_\parallel}$, the LVM's lie around 40 cm^{-1} *higher* in frequency than isolated Cu_{Zn}—$H_{BC_\parallel}$. We view the calculated upward shift in LVM frequency both as lending support to the model for the Cu-I band (and sidebands) and the related model for the EPR spectrum-III of Zwingel.[51]

The model proposed for spectrum-II[44,51] consisting of Cu_{Zn}—$Cu_i(T)$ pair trapping a single hydrogen was also investigated (Fig. 10). This relates to a center axially symmetric about the *c* axis. However, this structure proved to be unstable, spontaneously rearranging in the same manner as the Cu_{Zn}—Cu_i structure,[75] which cannot be easily reconciled with the EPR data. Indeed, we examined a number of starting configurations but found no stable structure aligned along the *c* axis, as required for the spectrum-II EPR center.[51]

IV. DISCUSSION AND CONCLUSIONS

We have performed density-functional simulations of a range of TM-related centers in ZnO. Fe, Co, Ni, and Cu centers generally obey Hund's rule and may be responsible for *n*-type doping either directly or by trapping hydrogen donors. We find that isolated hydrogen is unlikely to be a stable source of *n*-type doping due to measured and calculated migration barriers of less than 0.2 eV. Although an

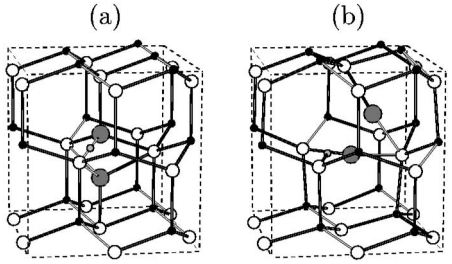

FIG. 10. Illustration of the (a) proposed Cu_{Zn}—$Cu_i(T)$—H_i structure and (b) the relaxed geometry obtained. The shading and axes are as described in Fig. 7, with H represented by the light gray ball.

equilibrium concentration of hydrogen will exist in pure ZnO, the presence of traps and hydrogen effusion may result in the loss of isolated hydrogen over time. Indeed a recent study[39] has shown that over-room-temperature anneals for several days lead to the loss of hydrogen-related LVM's correlated with the loss of free carriers. If H is mobile at low temperatures, this casts doubt over the assignment of the H-I and 3326.3-cm^{-1} IR bands to *isolated* interstitial H.[41,47] Indeed, we have no candidate for an H_{AB_O} center, since all impurity-H complexes we studied stabilize H_{BC} over H_{AB_O} by half an eV or more.

TM_{Zn} form preferentially over the TM_i in O-rich conditions. A detailed analysis of the electronic structure of these centers is complicated by the 3*d* bands of the impurity atoms. Due to the underestimate of the band gap inherent in local-density-approximation calculations, this leads to some ambiguity in the interpretation of the electrical character of these defects. However, by combining formation energies with band structure, the acceptor level of Cu_{Zn} can be explained, and the measured spin states of EPR-active centers are reproduced. In addition, TM-H complexes such as Cu_{Zn}—H_2 are stable shallow donor systems, which should be stable to room temperature, and we suggest that such trapped H, rather than isolated H_i, is responsible for at least some of the H-related donor activity. Indeed, several TM defects give rise to donor levels high in the band gap even in the absence of H, and our results suggest that such accidental contaminants would tend to enhance the as-grown *n*-type character even in the absence of hydrogen.

There is a clear trend for lower binding energies as the atomic number of the TM diminishes. This is in line with the observation of Cu—H complexes in FTIR studies with relatively high thermal stabilities and the lack of clear data for other TM-H complexes.

The local structure of most TM-H complexes can be described simply as perturbations of isolated, bond-centered H_i, and there is no direct interaction between the TM and H impurities; the similarity in frequencies reflects the role of the TM impurity purely as an elastic and electrostatic perturbation to the O—H group giving rise to the LVM's. This means that hydrogen-related IR modes for these complexes will not directly identify the TM, but the application of first-principles simulations may facilitate the assignment of experimentally observed centers. Our confidence is founded on the agreement with the Cu—I line at 3191.8 cm^{-1} for the stretch modes calculated for the Cu_{Zn}—H_i complex. Additionally, the upward shift in frequency for $Cu_{Zn,2}$—H_2 supports the model for the formation of these centers in material with large concentrations of Cu.[43]

Although the H modes do not reveal the TM species, we note that a range of low-frequency, pseudolocal modes associated with the TM impurities were also found, and if these could be detected experimentally and correlated with H-related modes, this should yield unambiguous evidence as to the microscopic structures involved.

The agreement between Cu_{Zn}—H_i and Cu—I contrasts with the lack of agreement between the H-I^* and O—H···Ni complex, which casts doubt over this model. However, our previously calculated[17] modes for O—H···Li and O—D···Li at 3556 and 2586 cm^{-1} are in very good agreement with H-I^* and support this revised model.[48,50] The calculated binding energy[16,17] of this center at 1.22–1.3 eV suggests that O—D···Li would dissociate around the lower limit (350 °C) of the annealing range of H-I^*,[48] given the uncertainty in the activation energy. Provided the defect responsible for the H-I^* band is not stable to temperatures significantly higher than 350 °C, we view such an assignment of H-I^* to O—H···Li_{Zn} as being consistent with theory.

However, if H-I^* is stable close to the upper limit of 1200 °C, the only type of center for which we predict there to be sufficiently high binding energy is V_{Zn}—H. Since there is no direct evidence for the presence of Li (or any other impurity) in the H-I^* spectra,[42,50] the correlation of the IR band with the presence of such impurities may be indicative of the Zn-lean growth conditions required for the formation of V_{Zn}—H defects. A more precise estimate of the thermal stability of H-I^* would certainly aid the assignment.

Additional hydrogen is less strongly bound to defect centers. This is particularly significant in the case of V_{Zn}, where the loss of the H-II band is associated with the loss of one hydrogen with an activation energy calculated at 2.1 eV. In addition, the calculated LVM's for the V_{Zn}—H_2 structure are in close agreement with the H-II bands of Lavrov, *et al.*[41] with an excellent agreement in isotopic shift.

H can be trapped at TM pairs, with Cu_{Zn}—Cu_{Zn}—H_i bound more tightly than Cu_{Zn}—Cu_i—H_i. The specific model proposed by Mollwo *et al.*[44] for Cu_{Zn}—Cu_i—H_i was found to be structurally unstable. It rearranges to form a Cu—Cu pair split across a Zn site (Cu_{Zn}—Cu_i) and a relatively unperturbed H_i bonded to an adjacent oxygen atom. This relaxed structure cannot account for the experimental observations.[44]

ACKNOWLEDGMENT

We would like to acknowledge the financial support of the Engineering and Physical Sciences Research Council (U.K.).

[1] J. H. Kim, H. Kim, D. Kim, Y. E. Ihm, and W. K. Choo, Physica B **327**, 304 (2003).

[2] K. Ando, H. Saito, Z. Jin, T. Fukumura, M. Kawasaki, Y. Matsumoto, and H. Koinuma, J. Appl. Phys. **89**, 7284 (2001).

[3] S.-W. Lim, D.-K. Hwang, and J.-M. Myoung, Solid State Commun. **125**, 231 (2003).

[4] K. Ueda, H. Tabata, and T. Kawai, Appl. Phys. Lett. **79**, 988 (2001).

[5] N. Jedrecy, H. J. von Bardeleben, Y. Zheng, and J-L. Cantin, Phys. Rev. B **69**, 041308(R) (2004).

[6] A. Hausmann and P. Schreiber, Solid State Commun. **7**, 631 (1969).

[7] W. M. Walsh and L. W. Rupp, Jr., Phys. Rev. **126**, 952 (1962).
[8] W. C. Holton, J. Schneider, and T. L. Estle, Phys. Rev. **133**, A1638 (1964).
[9] Y. Kanai, Jpn. J. Appl. Phys., Part 1 **30**, 703 (1991).
[10] H.-J. Schulz and M. Thiede, Phys. Rev. B **35**, 18 (1987).
[11] L. S. Vlasenko, G. D. Watkins, and R. Helbig, Phys. Rev. B **71**, 115205 (2005).
[12] R. Heitz, A. Hoffmann, and I. Broser, Phys. Rev. B **45**, 8977 (1992).
[13] O. F. Schirmer, J. Phys. Chem. Solids **29**, 1407 (1968).
[14] E. Tomzig and H. Helbig, J. Lumin. **14**, 403 (1976).
[15] B. K. Meyer, H. Alves, D. M. Hofmann, W. Kriegseis, D. Forster, F. Bertram, J. Christen, A. Hoffmann, M. Straßburg, M. Dworzak, U. Haboeck, and A. V. Rodina, Phys. Status Solidi B **241**, 231 (2004).
[16] E.-C. Lee and K. J. Chang, Phys. Rev. B **70**, 115210 (2004).
[17] M. G. Wardle, J. P. Goss, and P. R. Briddon, Phys. Rev. B **71**, 155205 (2005).
[18] K. Kobayashi, T. Maeda, S. Matsushima, and G. Okada, J. Mater. Sci. **27**, 5953 (1992).
[19] Z. Yin, N. Chen, C. Chai, and F. Yang, J. Appl. Phys. **96**, 5093 (2004).
[20] H.-J. Lee, S.-Y. Jeong, C. R. Cho, and C. H. Park, Appl. Phys. Lett. **81**, 4020 (2002).
[21] A. S. Risbud, N. A. Spaldin, Z. Q. Chen, S. Stemmer, and R. Seshadri, Phys. Rev. B **68**, 205202 (2003).
[22] D. P. Norten, M. E. Overberg, S. J. Pearton, K. Prussner, J. D. Budai, L. A. Boatner, M. F. Chisholm, J. S. Lee, Z. G. Khim, Y. D. Park, and R. G. Wilson, Appl. Phys. Lett. **83**, 5488 (2003).
[23] Y. Zheng, J. C. Boulliard, D. Demaille, Y. Bernard, and J. F. Pétroff, J. Cryst. Growth **274**, 156 (2005).
[24] F. Oba, T. Yamamoto, Y. Ikuhara, I. Tanaka, and H. Adachi, Microelectron. J. **43**, 1439 (2002).
[25] T. Aoki, Y. Hatanaka, and D. C. Look, Appl. Phys. Lett. **76**, 3257 (2000).
[26] A. B. M. Ashrafi, I. Suemune, H. Kumano, and S. Tanaka, Jpn. J. Appl. Phys., Part 2 **41**, L1281 (2002).
[27] K.-H. Bang, D.-K. Hwang, M.-C. Park, Y.-D. Ko, I. Yun, and J.-M. Myoung, Appl. Surf. Sci. **210**, 177 (2003).
[28] X.-L. Guo, H. Tabata, and T. Kawai, J. Cryst. Growth **223**, 135 (2001).
[29] K.-K. Kim, H.-S. Kim, D.-K. Hwang, J.-H. Lim, and S.-J. Park, Appl. Phys. Lett. **83**, 63 (2003).
[30] D. C. Look and B. Claffin, Phys. Status Solidi B **241**, 624 (2004).
[31] K. Minegishi, Y. Koiwai, Y. Kikuchi, and K. Yano, Jpn. J. Appl. Phys., Part 2 **36**, L1453 (1997).
[32] Y. R. Ryu, T. S. Lee, and H. W. White, Appl. Phys. Lett. **83**, 87 (2003).
[33] C. G. Van de Walle, Phys. Rev. Lett. **85**, 1012 (2000).
[34] S. F. J. Cox, E. A. Davis, S. P. Cottrell, P. J. C. King, J. S. Lord, J. M. Gil, H. V. Alberto, R. C. Vilão, J. Piroto Duarte, N. Ayres de Campos, A. Weidinger, R. L. Lichti, and S. J. C. Irvine, Phys. Rev. Lett. **86**, 2601 (2001).
[35] D. M. Hofmann, A. Hofstaetter, F. Leiter, H. Zhou, F. Henecker, B. K. Meyer, S. B. Orlinskii, J. Schmidt, and P. G. Baranov, Phys. Rev. Lett. **88**, 045504 (2002).
[36] D. C. Look, C. Coşkun, B. Claflin, and G. C. Farlow, Physica B **340-342**, 32 (2003).
[37] D. C. Look, J. W. Hemsky, and J. R. Sizelove, Phys. Rev. Lett. **82**, 2552 (1999).
[38] K. Ip, M. E. Overberg, Y. W. Heo, D. P. Norton, S. J. Pearton, C. E. Stutz, B. Luo, F. Ren, D. C. Look, and J. M. Zavada, Appl. Phys. Lett. **82**, 385 (2003).
[39] S. J. Jokela and M. D. McCluskey, Phys. Rev. B **72**, 113201 (2005).
[40] F. G. Gartner and E. Mollwo, Phys. Status Solidi B **89**, 381 (1978).
[41] E. V. Lavrov, J. Weber, F. Börrnert, C. G. Van de Walle, and R. Helbig, Phys. Rev. B **66**, 165205 (2002).
[42] E. V. Lavrov, Physica B **340-342**, 195 (2003).
[43] F. G. Gartner and E. Mollwo, Phys. Status Solidi B **90**, 33 (1978).
[44] E. Mollwo, G. Müller, and D. Zwingel, Solid State Commun. **15**, 1475 (1974).
[45] S. J. Jokela, M. D. McCluskey, and K. G. Lynn, Physica B **340-342**, 221 (2003).
[46] C. H. Seager and S. M. Myers, J. Appl. Phys. **94**, 2888 (2003).
[47] M. D. McCluskey, S. J. Jokela, K. K. Zhuravlev, P. J. Simpson, and K. G. Lynn, Appl. Phys. Lett. **81**, 3807 (2002).
[48] E. V. Lavrov, F. Börrnert, and J. Weber, Phys. Rev. B **71**, 035205 (2005).
[49] N. H. Nickel and K. Fleischer, Phys. Rev. Lett. **90**, 197402 (2003).
[50] L. E. Halliburton, L. Wang, L. Bai, N. Y. Garces, N. C. Giles, M. J. Callahan, and B. Wang, J. Appl. Phys. **96**, 7168 (2004).
[51] D. Zwingel, Phys. Status Solidi B **67**, 507 (1975).
[52] R. Jones and P. R. Briddon, in *Identification of Defects in Semiconductors*, Vol. 51A of *Semiconductors and Semimetals*, edited by M. Stavola (Academic, Boston, 1998), Chap. 6.
[53] N. Troullier and J. L. Martins, Phys. Rev. B **43**, 1993 (1991).
[54] H. J. Monkhorst and J. D. Pack, Phys. Rev. B **13**, 5188 (1976).
[55] A. F. Kohan, G. Ceder, D. Morgan, and Chris G. Van de Walle, Phys. Rev. B **61**, 15019 (2000).
[56] F. Oba, S. R. Nishitani, S. Isotani, and H. Adachi, J. Appl. Phys. **90**, 824 (2001).
[57] S. B. Zhang and J. E. Northrup, Phys. Rev. Lett. **67**, 2339 (1991).
[58] G. Makov and M. C. Payne, Phys. Rev. B **51**, 4014 (1995).
[59] J. A. Dean, *Lange's Handbook of Chemistry*, 15th ed. (McGraw-Hill, New York, 1999).
[60] $E^b(AB) = E^f(A) + E^f(B) - E^f(AB)$.
[61] R. Jones, J. Goss, C. Ewels, and S. Öberg, Phys. Rev. B **50**, 8378 (1994).
[62] C. G. Van de Walle and J. P. Goss, Mater. Sci. Eng., B **58**, 17 (1999).
[63] S. Limpijumnong and S. B. Zhang, Appl. Phys. Lett. **86**, 151910 (2005).
[64] C. H. Park and D. J. Chadi, Phys. Rev. Lett. **94**, 127204 (2005).
[65] G. F. Koster, in *Space Groups and Their Representations*, Vol. 5 of *Solid State Physics*, edited by F. Seitz and D. Turnbull (Academic, New York, 1957).
[66] P. W. Peacock and J. Robertson, Appl. Phys. Lett. **83**, 2025 (2003).
[67] Ç. Kiliç and A. Zunger, Appl. Phys. Lett. **81**, 73 (2002).
[68] A. Zunger, Appl. Phys. Lett. **83**, 57 (2003).
[69] S. Kolesnik, B. Dabrowski, and J. Mais, J. Appl. Phys. **95**, 2582 (2004).
[70] Z.-W. Jin, T. Fukumura, K. Hasegawa, Y. Z. Yoo, K. Ando, T. Sekiguchi, P. Ahmet, T. Chikyow, T. Hasegawa, H. Koinuma, and M. Kawasaki, J. Cryst. Growth **237-239**, 548 (2002).

[71] X. Feng, J. Phys.: Condens. Matter **16**, 4251 (2004).
[72] W. D. Kingery, H. K. Bowen, and D. R. Uhlmann, *Introduction to Ceramics* (Wiley, New York, 1975).
[73] P. T. Huy and C. A. J. Ammerlaan, Phys. Rev. B **66**, 165219 (2002).
[74] B. Hourahine, R. Jones, S. Öberg, P. R. Briddon, and T. Frauenheim, Physica B **340-432**, 668 (2003).
[75] M. G. Wardle, J. P. Goss, and P. R. Briddon (unpublished).